Journal of Magnetic Resonance 207 (2010) 197–205

Contents lists available at ScienceDirect

Journal of Magnetic Resonance

journal homepage: www.elsevier.com/locate/jmr

Characteristics of zero-quantum correlation spectroscopy in MAS NMR experiments

Stephanie G. Köneke, Jacco D. van Beek, Matthias Ernst, Beat H. Meier *

ETH Zürich, Physical Chemistry, Wolfgang-Pauli-Strasse 10, 8093 Zürich, Switzerland

ARTICLE INFO

Article history:
Received 24 June 2010
Revised 29 August 2010

Keywords:
NMR
Multi-quantum coherence
Zero-quantum coherence
Magic-angle spinning
Recoupling

ABSTRACT

Zero-quantum coherence generation and reconversion in magic-angle spinning solid-state NMR is analyzed. Two methods are discussed based on implementations using symmetry-based pulse sequences that utilize either isotropic *J* couplings or dipolar couplings. In either case, the decoupling of abundant proton spins plays a crucial role for the efficiency of the zero-quantum generation. We present optimized sequences for measuring zero-quantum single-quantum correlation spectra in solids, achieving an efficiency of 50% in ubiquitin. The advantages and disadvantages of zero-quantum single-quantum over single-quantum single-quantum correlation spectroscopy are explored, and similarities and differences with double-quantum single-quantum correlation spectroscopy are discussed. Finally, possible application of zero-quantum single-quantum experiments to polypeptides, where it can lead to better spectral resolution is investigated using ubiquitin, where we find high efficiency and high selectivity, but also increased line widths in the MQ dimension.

1. Introduction

Two-dimensional (2D) chemical-shift correlation spectroscopy [1] is an important tool for the resonance assignment of NMR spectra and for the elucidation of structural or chemical information in many applications with inorganic, organic, and biological solids. Under magic-angle spinning (MAS) conditions, either isotropic *J* couplings or dipolar couplings can be utilized to characterize the topology of spin systems. In the context of single-quantum single-quantum (SQ) correlation spectroscopy, these interactions are used as the driving force for polarization transfer in the mixing time of the 2D experiment [2], while, in zero-quantum (ZQ)–SQ or double-quantum (DQ)–SQ experiments, ZQ or DQ coherence is excited and evolves during t_1 before it is reconverted to SQ coherence for detection [3,4].

The SQ–SQ correlation spectra often lead to the most intuitive representation where the polarization-transfer step can be described by a master equation. The 2D cross-peak pattern is closely related to the corresponding kinetic matrix [5,6]. Nevertheless, correlation spectra with a multiple-quantum (MQ) dimension may be useful because they do not contain intense diagonal peaks. In homonuclear correlation spectra such diagonal peaks can be quite dominant and mask cross-peaks that contain the desired information, especially for spins with small chemical-shift differences that would appear close to the diagonal in SQ–SQ correlation spectra [7]. Furthermore, in the context of complex spectra, the spectral dispersion in ZQ–SQ or DQ–SQ correlation spectra may be favorable compared to SQ–SQ spectra [8]. In particular, ZQ coherences are expected to be independent of B_0-field inhomogeneities [9], which could lead to narrower lines in the ZQ dimension compared to a SQ dimension. Finally, spectra containing ZQ or DQ dimensions may be easier to implement in the context of resolution enhancement by spin-state selection [10–12].

Homonuclear chemical-shift correlation spectroscopy can either be based on pulse sequences generating an effective zero-quantum Hamiltonian (*J* coupling or dipolar-coupling based) or on pulse sequences generating an effective double-quantum Hamiltonian (dipolar-coupling based). Both methods have been extensively used for polarization transfer in the mixing time of SQ–SQ correlation spectroscopy. *J* coupling based ZQ polarization transfer has been implemented using the TOBSY pulse sequences [13–16] where all interactions except the homonuclear *J* couplings are suppressed. Dipolar-coupling based ZQ polarization transfer was employed in rotational resonance [17–19], RFDR [20,21], RIL [22,23] and using symmetry-based C or R sequences [24,25]. Dipolar-coupling based DQ polarization transfer was achieved using HORROR [26] or DREAM [27], DRAMA [28], BABA [29,30], C7 [31–33], and formulated in a more general way using symmetry-based C or R sequences [25,34–38]. Some sequences like DRAWS [39] generate a mixed ZQ/DQ effective Hamiltonian. Multiple-quantum–SQ correlation spectroscopy has so far been implemented mostly using DQ coherences with only a few ZQ–SQ spectra in liquids reported in the literature [40,41].

In this contribution we describe optimized experimental schemes to acquire two-dimensional ZQ–SQ experiments in solid-state NMR under MAS by using symmetry-based pulse sequences for the conversion between ZQ and SQ coherences. The

* Corresponding author.
E-mail address: beme@ethz.ch (B.H. Meier).

1090-7807/$ - see front matter © 2010 Elsevier Inc. All rights reserved.
doi:10.1016/j.jmr.2010.08.020

first sequence for generating an effective ZQ Hamiltonian discussed here, POST-C9$^1_6$ [15], is based on isotropic *J* couplings while the second sequence, SR6$^2_6$ [24], is based on dipolar couplings. We present the superior excitation and reconversion efficiency of ZQ coherences for the *J* coupling, reaching up to 90% experimental efficiency in a two-spin system, which is higher than the DQ efficiencies achieved for the POST C7$^1_2$ [35] and the SC14$^5_4$ sequences [34]. The efficiency of proton decoupling, which we find to be a complex function of the decoupling field strength, turns out to be critical for the efficiency of MQ excitation. The number of peaks that can be resolved by ^{13}C–^{13}C two-dimensional ZQ–SQ experiments were found to be comparable for DQ–SQ and ZQ–SQ experiments in the model protein ubiquitin.

2. Properties of MQ–SQ correlation spectra

Multiple-quantum single-quantum correlation spectra are based on pulse sequences that generate an effective DQ or ZQ Hamiltonian. The experimental implementation and the properties of DQ–SQ correlation spectra are well established but there are only a few experimental realizations of ZQ–SQ correlation spectra [40,42]. In this section we discuss a number of points that need to be taken into account when recording MQ–SQ correlation spectra. In particular the experimental realization of ZQ–SQ spectra is discussed in detail.

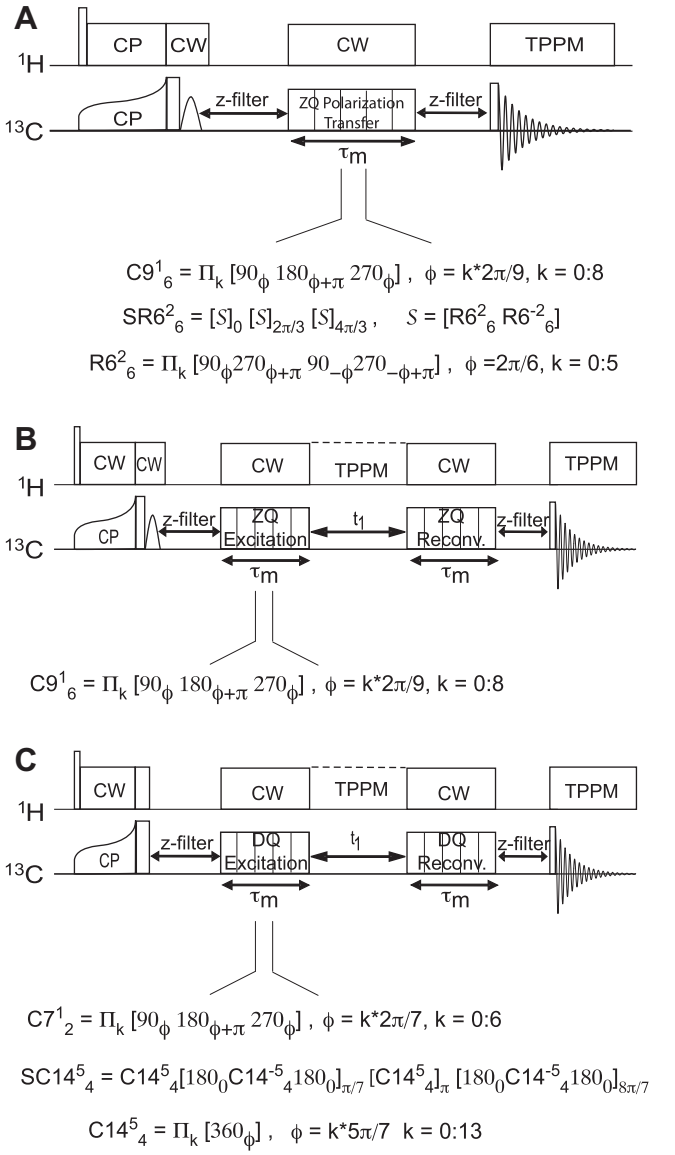

Fig. 1. Pulse sequences used for (A) determining ZQ transfer efficiency, (B) measuring 2D ZQ–SQ correlation spectra and (C) measuring 2D DQ–SQ correlation spectra. The notation $[\cdots]_\phi$ indicates an overall phase shift of the sequence in the bracket by ϕ. All flip angles are given in degree and phases in radians.

The pulse sequences shown in Fig. 1B and C follow the general scheme of 2D correlation experiments, i.e., a MQ state is prepared, then evolved during t_1, after which it is reconverted to SQ coherences for detection. In contrast to measuring SQ–SQ and DQ–SQ correlation spectra, which start with an initial condition proportional to sum polarization, e.g., from a thermal-equilibrium state, ZQ–SQ spectra require an initial condition of difference polarization [40,42] (I_{1z}-I_{2z}) in order for ZQ coherences ($I_1^+I_2^- - I_1^-I_2^+$) to be excited. This is a consequence of the fact that the sum polarization commutes with the ZQ Hamiltonian and, thus, does not evolve under it. Generating difference polarization can, for example, be achieved with a band-selective pulse to invert one or a particular group of resonances. Such an approach will always lead to selective ZQ spectra where pairs of resonances that have no initial difference polarization will not produce a signal in the 2D ZQ–SQ correlation spectrum. In reality, the behavior is more complicated due to differences in the cross-polarization efficiency and due to multi-spin effects (*vide infra*). Fig. 2 shows a schematic drawing of the expected peaks in a 2D ZQ–SQ correlation spectrum of a three-spin system where resonance two has been inverted and the initial intensity was equal for all spins. For each pair of SQ resonances, δ_n and δ_m, two cross peaks with opposite sign are expected at the ZQ frequency $|\delta_n - \delta_m|$ (large circles in Fig. 2), although other cross peaks are often also found due to relay effects (small circles in Fig. 2).

The ZQ coherences $I_1^+I_2^- - I_1^-I_2^+$ can be excited from initial difference polarization using either the dipolar interaction or the isotropic *J* coupling, with a choice of many recoupling sequences under MAS from the literature [13–15,17–25]. *J*-coupling based sequences generate an isotropic ZQ Hamiltonian that allows a transfer efficiency of up to 100%, neglecting relaxation effects, at the cost of longer mixing times in the order of 10 ms due to the small magnitude of the homonuclear *J* couplings. Using dipolar-coupling based sequences restricts the efficiency to 71% for γ-encoded sequences but the mixing times will be significantly shorter (in the

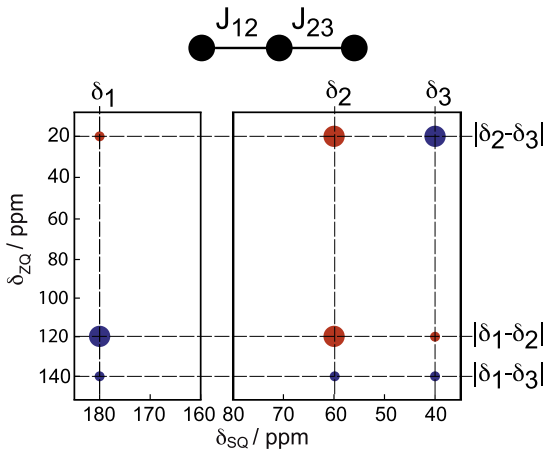

Fig. 2. Schematic drawing of a 2D ZQ–SQ correlation spectrum. Resonances are specified with two labels, the first representing the SQ frequency δ_n, the second representing the ZQ frequency as the difference of the SQ frequencies $|\delta_n - \delta_m|$. Red denotes negative and blue positive signals. The small circles denote relay peaks. (For interpretation of the references to colour in this figure legend, the reader is referred to the web version of this article.)

order of 1 ms) due to the larger magnitude of the homonuclear dipolar couplings. The isotropic *J*-coupling based Hamiltonian allows arbitrary dwell times during the t_1 evolution. For the dipolar-coupling based supercycled sequence $SR6_6^2$, however, the complex phase-time relationships [25] that need to be taken into account for sub-cycle dwell times, severely complicates having a spectral width in the indirect dimension larger than the spinning frequency.

For an efficient MQ excitation the rf-field amplitude of the proton decoupling during the excitation and reconversion sequence was found to be one of the most important factors [36,38,43]. At rf-field amplitudes that are typically accessible using commercial MAS probes, a multitude of destructive resonance conditions must be avoided in order to generate the desired effective ZQ or DQ Hamiltonian and to minimize other terms. Typically, it was found for DQ sequences, the proton rf-field amplitude has to be three times the S-spin rf-field amplitude in order to obtain good polarization transfer, independent of the exact setting of the proton rf-field amplitude [36,38,43]. At high spinning frequencies, MQ excitation without proton decoupling is more efficient and easier to implement than high-power decoupling, especially for temperature-sensitive samples. This is consistent with previous observations made with DQ sequences like $POST\text{-}C7_2^1$ as well as R sequences [37,38].

The resulting line width in the MQ dimension of MQ–SQ correlation spectra is an important factor whether such experiments can contribute significantly to the resonance assignment of complex system, e.g., biological macromolecules. Depending on the degree of correlation of the line-broadening mechanisms at the two spins involved, one would expect differences in the line width in the

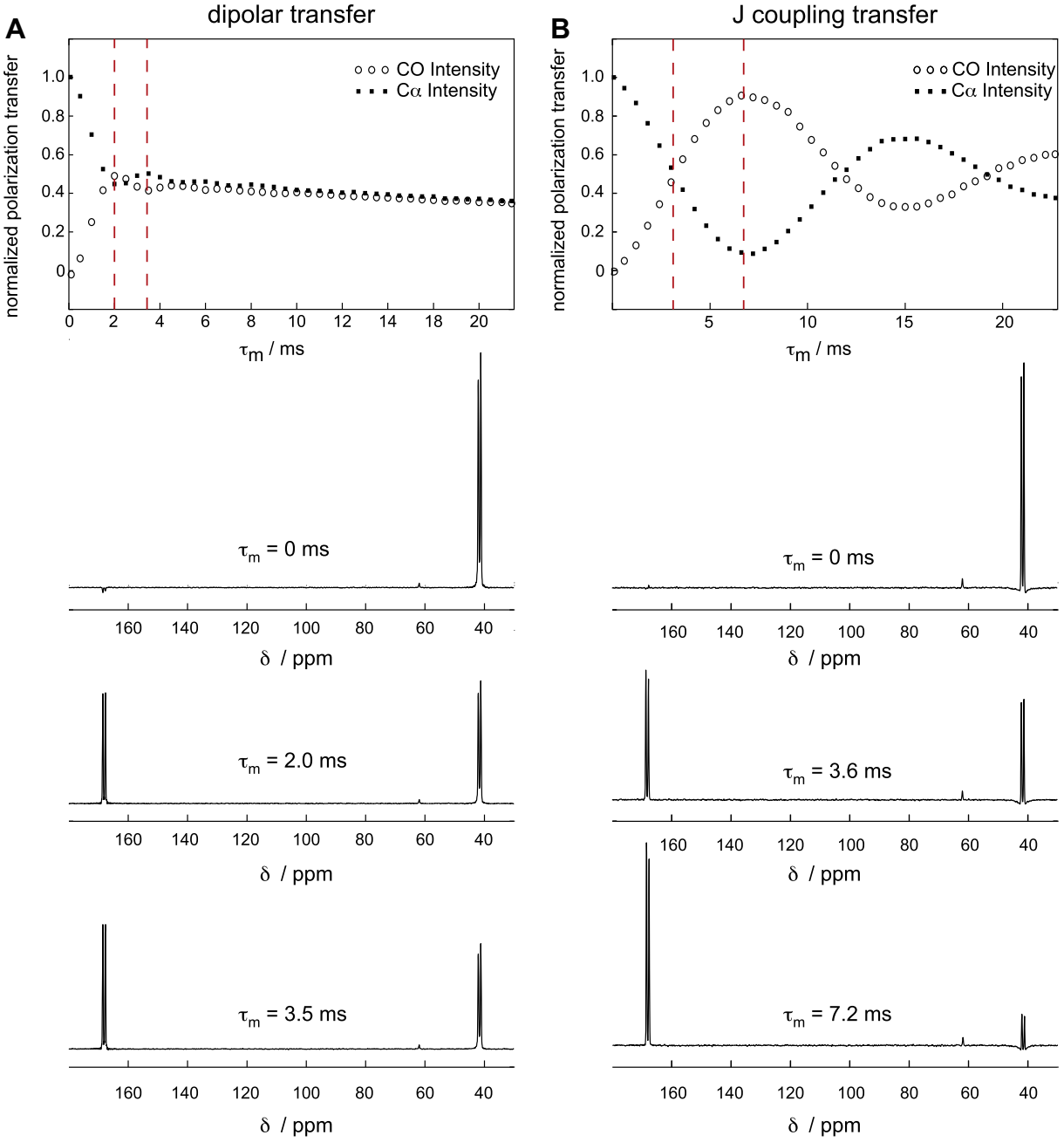

Fig. 3. ZQ polarization-transfer efficiency at $B_0 = 7$ T as a function of the mixing interval τ_m, measured for $^{13}C_2$, ^{15}N glycine ethyl ester using (A) $SR6_6^2$ at 24 kHz MAS or (B) $POST\text{-}C9_6^1$ at 20 kHz MAS.

indirect dimension. If the line broadening is fully uncorrelated, the DQ and ZQ line width would be roughly the sum of the two SQ line widths. If the line broadening of the two SQ lines is fully correlated, as one would expect in the case that the line width is dominated by B_0-field inhomogeneities, the ZQ line width would be significantly narrower than the SQ lines while the DQ line would be broader. In the case of anti correlation of the line-broadening mechanisms of the two SQ lines, the DQ lines would be narrower while the ZQ lines would be broader than the two SQ lines [44,45].

Finally, it is interesting to consider MQ–SQ correlation spectra as an alternative to SQ–SQ spectra to obtain additional spectral resolution in crowded 2D spectra, e.g., of proteins. It was pointed out by Luca and Baldus [8] that the correlation of a MQ with a SQ dimension has advantages in terms of spectral resolution in protein spectra because the isotropic chemical shifts for CO, C_α and C_β are correlated in proteins when comparing resonances from different secondary structure elements. For example, the shifts of C_α and C_β resonances are anti-correlated when comparing α-helix and β-sheet elements while the shift of C_α and C′ resonances are correlated [46]. In Ref. [8] correlation spectra with sum and difference frequencies (but without generating MQ coherences) have been recorded and their usefulness in certain cases has been demonstrated. Here we investigate MQ–SQ correlation spectra that suppress the diagonal signals which leads to further spectral enhancement due to the suppression of auto-correlation peaks.

3. Experimental details

All experiments on $^{13}C_2$,^{15}N glycine ethyl ester, U-^{13}C,^{15}N valine–phenylalanine, and U-^{13}C,^{15}N arginine were performed at a B_0 field of 7 T using a Varian Infinity + 300 spectrometer and a Varian 2.5 mm double-resonance probe, experiments on ubiquitin on a Varian Infinity + 500 spectrometer using a 1.8 mm double-resonance probe [47]. An actively-switched preamplifier was used to allow soft pulses without truncation at low rf-field amplitudes. Typical experimental parameters included cross-polarization intervals of 2 ms (1.3 ms for ubiquitin), z-filter delays of 5 ms, recycle delays of 3 s (5 s for ubiquitin), 90° pulse lengths of 2.5 μs for both ^{13}C and ^{1}H. TPPM [41] decoupling was used in the free evolution periods of the 2D experiments with 120 kHz proton rf-field amplitude. For the selective inversion an IBURP-2 [48] pulse was used with a length of 3 ms. Phase transients were carefully minimized for the ^{13}C channel by adjusting the length of the transmitter cable. For the different pulse sequences the ratios between ^{13}C rf-field amplitude and the spinning frequency were 3, 2, 7 and 3.5 for the POST-C9$^1_6$ [15], SR6$^2_6$ [24], POST-C7$^1_2$ [31] and SC14$^4_5$ [34] sequences, respectively. The experimentally-determined optimum values were close to the theoretical ratios. The t_1 evolution was 6.4 ms and the t_2 acquisition was 40.9 ms. For DQ excitation and reconversion in ubiquitin, the SC14$^5_4$ sequence was used with 140 kHz ^{13}C field amplitude and for ZQ excitation and reconversion the POST-C9$^1_6$ sequence with 120 kHz rf-field amplitude. No proton decoupling was applied during the two pulse sequences. All data processing was done using matNMR [49]. U-$^{13}C_2$,^{15}N glycine ethyl ester, U-$^{13}C_2$,^{15}N valine–phenylalanine were custom synthesized and recrystallized. U-^{13}C,^{15}N arginine was purchased from Cambridge Isotopes and used as is. U-^{13}C,^{15}N ubiquitin was expressed in *Escherichia coli* and crystallized as described in Ref. [50].

4. Results and discussion

To determine the efficiency of ZQ recoupling, the pulse sequence shown in Fig. 1A was used to measure the polarization-transfer efficiency in a two-spin system. After cross polarization, one of the two lines in $^{13}C_2$–^{15}N-labeled glycine ethyl ester was put in the x/y plane by a selective pulse and dephased during the z-filter period. The evolution of the initial polarization difference was then observed under the ZQ pulse sequence with simultaneous cw proton decoupling. Fig. 3 shows the ZQ efficiency for the dipolar-coupling based SR6$^2_6$ sequence at a spinning frequency of 24 kHz (Fig. 3A) and for the J-coupling based POST-C9$^1_6$ sequence at a spinning frequency of 20 kHz (Fig. 3B). The efficiency was detected by observing the polarization transfer from the C_α to the CO resonance using ^{13}C rf-field amplitudes of 48 kHz and 60 kHz, respectively.

As expected, for the SR6$^2_6$ sequence the polarization was rapidly transferred to the CO due to the large magnitude of the one-bond dipolar coupling. Due to the anisotropic nature of the dipolar coupling and the distribution of the observed frequencies in the powder, the oscillations are strongly damped and a uniform distribution of the polarization was quickly reached. The maximum transfer was 46% of the initial polarization and was reached after a mixing time of 3.6 ms. The J-coupling based POST-C9$^1_6$ sequence shows a damped oscillatory transfer with a first maximum at 90% of the initial polarization after a mixing time of 7.2 ms, cor-

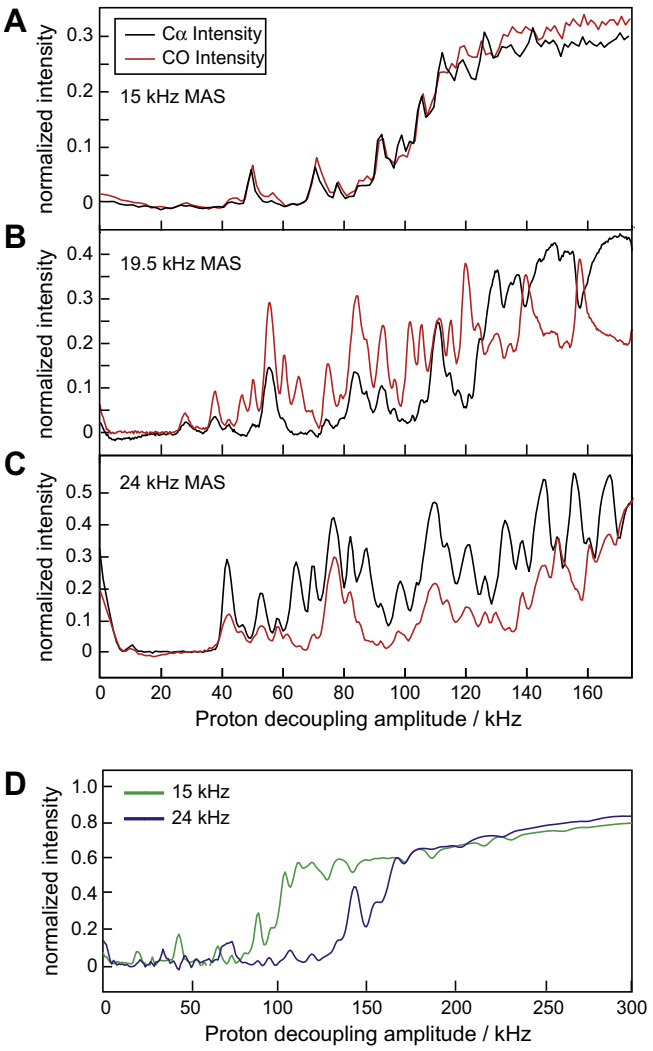

Fig. 4. (A–C) Experimental ZQ efficiency obtained for $^{13}C_2$, ^{15}N glycine ethyl ester at B_0 = 7T and τ_m = 7.2 ms, as a function of CW proton decoupling amplitude using (A) 15 kHz, (B) 19.5 kHz and (C) 24 kHz MAS. Plotted are the integrated peak intensities, normalized to data obtained for τ_m = 0 ms. (D) shows a numerical simulation of the sequence applied to a system C–C–H_2 (with geometry of glycine ethyl ester).

responding to an approximate value of the *J*-coupling constant of 69 Hz. The damping is in this case due to dipolar contributions to the zero-quantum Hamiltonian or due to relaxation processes. The value of the *J* coupling extracted from these experiments is somewhat larger than the experimentally determined value from the splitting of 64 Hz observed in 1D spectra of glycine ethyl ester and this points to non-idealities of the pulse sequence. As noted above, the efficiency of the proton decoupling is one important reason for deviations of the effective coupling strength compared to the theoretical *J*-coupling. In our example, the POST-C9$_6^1$ sequence clearly resulted in better polarization-transfer efficiency than the dipolar SR6$_6^2$ sequences despite the longer mixing time. For comparison, we also measured the efficiency of the DQ polarization transfer using the C7$_2^1$ sequence at a spinning frequency of 20 kHz, which reached a maximum of 35% of the initial polarization at a mixing time of 0.7 ms.

Fig. 4A–C shows experimental ZQ excitation and reconversion efficiencies obtained for $^{13}C_2$, ^{15}N glycine ethyl ester using the POST-C9$_6^1$ sequence, as a function of the cw-decoupling amplitude for a fixed excitation and reconversion time of 7.2 ms. A one-dimensional version of the ZQ pulse sequence of Fig. 1B (t_1 = 0 ms) was used for three different spinning frequencies and proton rf-field amplitudes of up to 170 kHz. At 15 kHz MAS a large range with proton rf-field amplitudes below 100 kHz shows almost no transfer. At higher B_1 fields a rapid increase to a stable plateau is observed for rf-field amplitudes of 120 kHz or more. At higher spinning frequencies, the transition to a stable plateau value shifts to significantly higher rf-field amplitudes (Fig. 4B) or is even outside the observed range (Fig. 4C). In an intermediate range of decoupling field strengths a strong and irregular dependence on the rf-field amplitude is observed. The general behavior shown in Fig. 4 was found to be typical. Only the details were found to vary between different compounds and pulse sequences.

In order to obtain a basic understanding of this behavior, numerical simulations using the geometry of the C–C–H_2 four-spin system of glycine ethyl ester were performed using the GAMMA

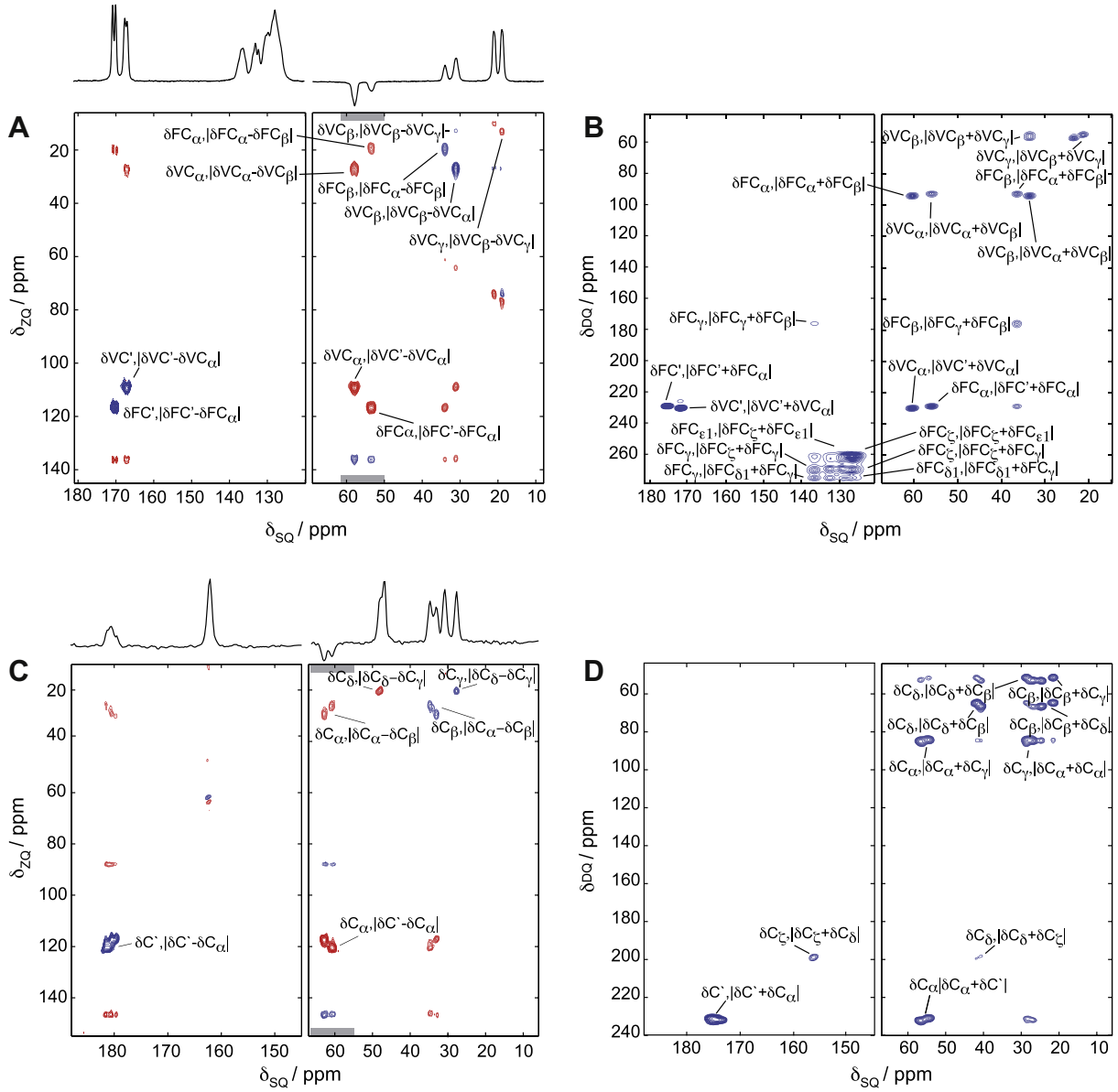

Fig. 5. 2D ZQ–SQ and 2D DQ–SQ spectra of (A and B) U-^{13}C, ^{15}N valine–phenylalanine and (C and D) U-^{13}C, ^{15}N arginine, recorded at B_0 = 7T and 20 kHz MAS. ZQ–SQ spectra were acquired using POST-C9$_6^1$ and τ_m = 3.6 ms (A), and τ_m = 4.2 ms (C), DQ–SQ spectra with C7$_2^1$ and τ_m = 0.3 ms. The total t_1 evolution was 6.4 ms for all spectra. The bandwidth of the inversion pulse used for the ZQ–SQ spectra is marked in grey. The scaling factor of the contour levels is 1.3 for all spectra.

C++ spin-simulation library [51] employing time slicing. The following parameters were used for the simulation: J-coupling constant between the S-spins $\delta_J = 50$ Hz, dipolar coupling constant $\delta_D = 4.2$ kHz, CSA $\delta_{S1} = -8$ kHz and CSA $\delta_{S2} = 8$ kHz. The J coupling between the I and the S spin was $\delta_J = 150$ Hz, the dipolar coupling constant between the protons was taken to be $\delta_D = 46$ kHz. Starting from an initial density operator $\sigma(0) = S_{1z}$ the polarization transfer to S_{2z} is calculated under the POST-C9$_6^1$ sequence [15]. The basic features of the experimental data are reproduced in Fig. 4D, but the detailed structure of the curves cannot be reproduced with such a simple model. A stable plateau was only observed for very high proton rf-field amplitudes (>160 kHz). This is beyond what can realistically be used on many commercial probes, especially for temperature-sensitive samples. Great care must therefore be used in the selection of the decoupling amplitude and careful experimental optimization is required for each spinning frequency and pulse sequence. Choosing the highest available rf-field is not necessarily the best choice.

To test the implementation of a 2D ZQ–SQ chemical-shift correlation experiment we applied the sequence of Fig. 1B to U-^{13}C,^{15}N valine–phenylalanine (Val-Phe) and to U-^{13}C,^{15}N arginine, and compared the results to DQ–SQ experiments (Fig. 5). For the generation of DQ coherence we used the POST-C7$_2^1$ sequence at 20 kHz MAS with 120 kHz ^{13}C rf-field amplitude, while for ZQ coherence generation the POST-C9$_6^1$ sequence was used at 20 kHz MAS with 60 kHz ^{13}C rf-field amplitude. The proton decoupling power during the POST-C9$_6^1$ sequence was 170 kHz. For the ZQ–SQ correlation spectra, the C_α region was inverted by an selective IBURP-2 pulse [48] of 1.3 ms length. The inverted region is indicated by a grey area in the spectra of Fig. 5.

The DQ–SQ spectra show most of the resonances with intensities as expected from the 1D spectrum, with some of the smaller signals attributed to relayed transfer. In contrast, the ZQ–SQ spectra shows a much more pronounced distribution of signal intensities, with the strongest peaks at the $|\delta_{CO}-\delta_{C\alpha}|$ ZQ frequencies in both spectra. The arginine spectra show two sets of signals originating from two different crystal forms in the sample. From the inversion region, denoted by the grey area in the spectra, we expected mainly $|\delta_{CO}-\delta_{C\alpha}|$ and $|\delta_{C\alpha}-\delta_{C\beta}|$ ZQ frequencies. In both spectra we detected additional resonances at the ZQ frequencies $|\delta_{CO}-\delta_{C\beta}|$ and $|\delta_{C\beta}-\delta_{C\gamma}|$. They are either due to differences in the initial polarization after CP or due to multi-spin effects generated by relayed polarization transfer under the pulse sequence.

The experimental cross-peak intensities of the spectra shown in Fig. 5 can, to a large extent, be reproduced by simple numerical simulations that take into account only the J-coupling network of the model substances. Fig. 6 shows the simulated ZQ cross-peak intensities of the three amino acids, as a function of the length of the ZQ excitation interval. The colored symbols indicate the measured experimental intensities of the nine cross peaks. For the mixing times of 3.6 ms and 4.2 ms the experimental intensities are in good agreement with the simulations for the measurements on Val-Phe. Somewhat larger discrepancies were observed for arginine. Using the J couplings for arginine, i.e., $J_{CO,C\alpha} = 53.4$ Hz and

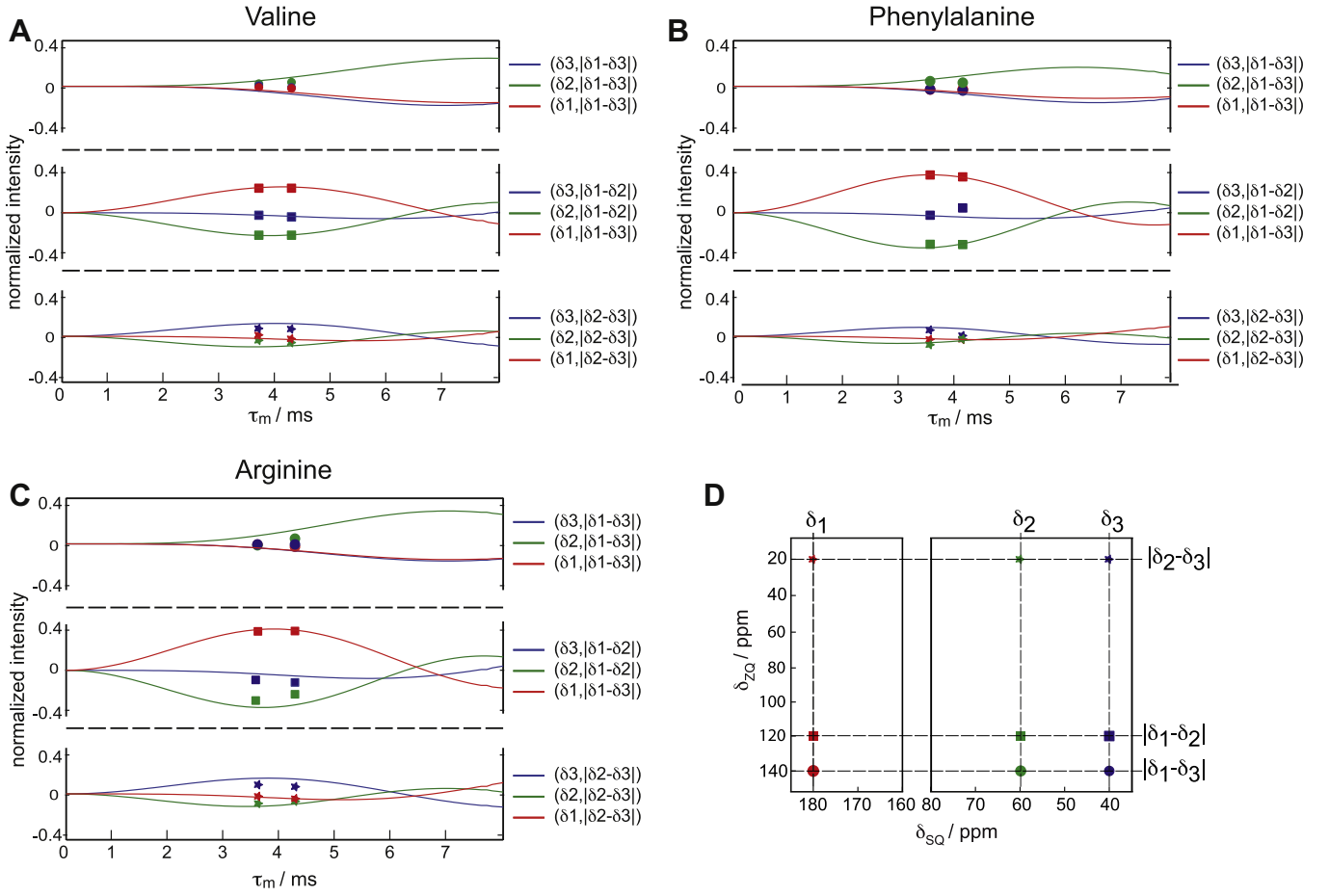

Fig. 6. Simulation of 2D ZQ–SQ spectra for various spin systems, as a function of the mixing interval τ_m. (A) Three-spin system with $J_{1,2} = 48$ kHz and $J_{2,3} = 35$ kHz. (B) Three-spin system with $J_{1,2} = 54$ Hz and $J_{2,3} = 19.5$ kHz. The system corresponds to values found for valine (A) phenylalanine (B) and arginine (C). Compared are the normalized intensities of the integrated resonances with intensities of the experimental spectra. The symbols, as explained in (D), denote the experimental intensities.

$J_{C\alpha,C\beta}$ = 34.3 Hz [42], the simulations show that at the excitation interval of 4.2 ms the observed (δ_{CO}, $|\delta_{CO}-\delta_{C\alpha}|$) and ($\delta_{C\alpha}$, $|\delta_{CO}-\delta_{C\alpha}|$) resonances are expected. The predicted intensities are in reasonable agreement to the experimental spectrum. The presence of (δ_x, $|\delta_{C\beta}-\delta_{C\gamma}|$) resonances, which appeared strongly despite being outside the inversion region, is indicative of a polarization difference caused through the CP condition.

To test the applicability of ZQ–SQ correlation spectra to a small model protein 2D ZQ–SQ spectrum (Fig. 7A) of a micro-crystalline sample of U-^{13}C,^{15}N ubiquitin at 40 kHz MAS were recorded. The C_α–CO region of the resulting spectrum was compared to a DQ–SQ spectrum (Fig. 7B) at 40 kHz MAS and a MIRROR-SD SQ–SQ [52] experiment taken at 40 kHz MAS (Fig. 7C). XIX [53] decoupling was used in the free evolution periods of the 2D experiments with 120 kHz proton rf-field amplitude. During the ZQ and DQ pulse sequences no proton decoupling was applied since this gave better efficiencies than decoupling with amplitudes still tolerable for a protein sample (<150 kHz). In terms of efficiency, the ZQ–SQ experiment is clearly the best: the 50% efficiency of the $|\delta_{CO}-\delta_{C\alpha}|$ resonances in the ZQ–SQ experiment was much higher than the

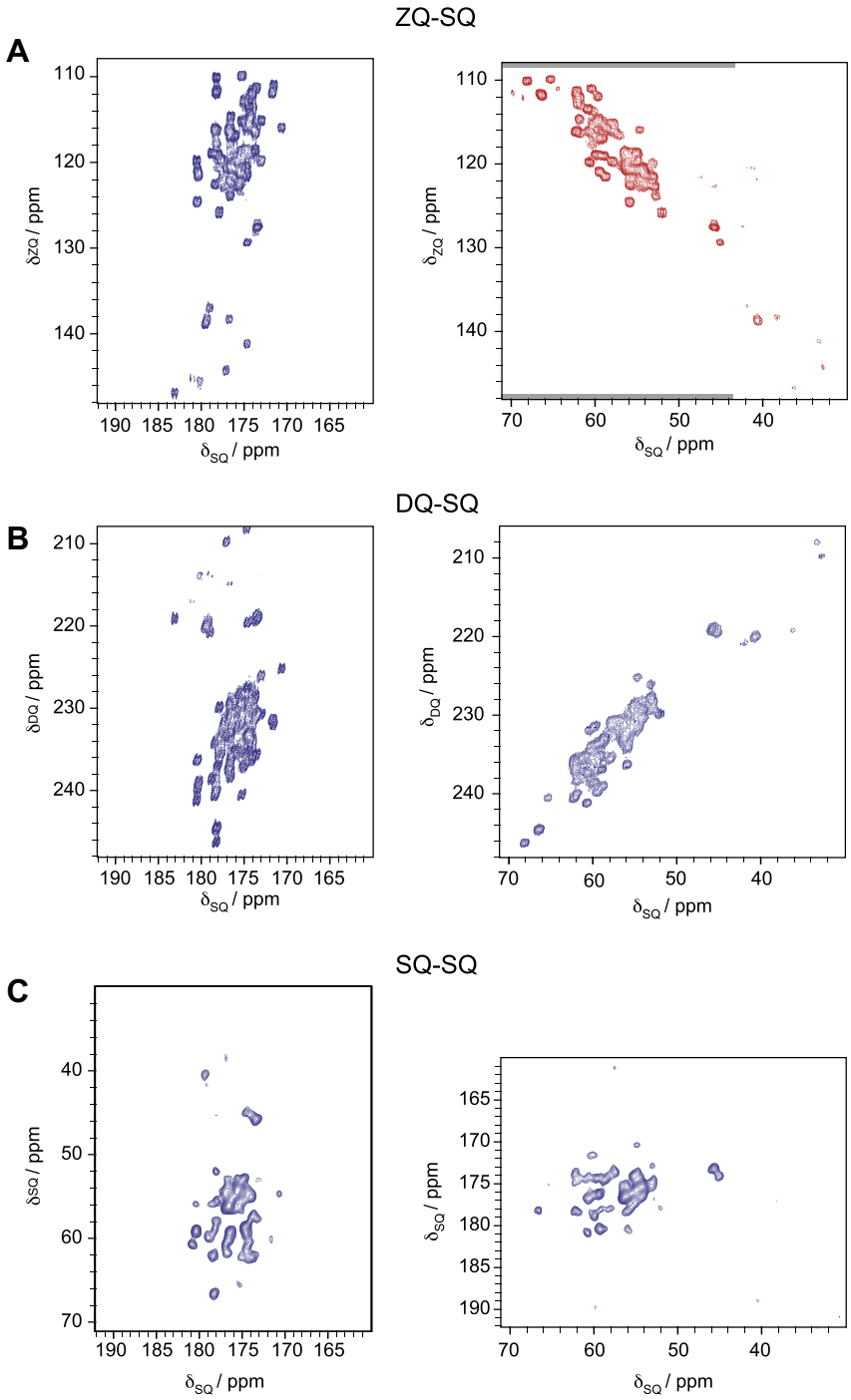

Fig. 7. Direct comparison of (A) ZQ–SQ, (B) DQ–SQ and (C) SQ–SQ correlation experiments, applied to U-^{13}C, ^{15}N ubiquitin at B_0 = 11.7 T. The ZQ–SQ spectrum was recorded with POST-C9$^1_6$, τ_m = 3.9 ms. The DQ–SQ spectrum was recorded with SC14$^5_4$, τ_m = 0.3 ms. The SQ–SQ spectrum was taken using a MIRROR–SD mixing interval of 12 ms and a cw rf-amplitude ν_1 of 16 kHz. All spectra were recorded at 40 kHz MAS. To allow comparison of the resolution in the indirect dimension, MQ–SQ spectra were acquired with a total t_1 evolution of 12.8 ms. The bandwidth of the inversion pulse used for the ZQ–SQ spectra is marked in grey. The 2D MIRROR–SD spectrum was taken from Ref. [52].

roughly 20% for the DQ–SQ experiment. In part this is due to the inherently higher efficiency of the *J*-coupling based POST-C9$^1_6$ sequence compared to γ-encoded dipolar sequences, but also differences in the decoupling properties of ZQ and DQ sequences may play a role. No $|\delta_{C\alpha}-\delta_{C\beta}|$ resonances were observed in the ZQ–SQ experiment, which we ascribe to the less-than-perfect decoupling without proton irradiation. A few $|\delta_{CO}-\delta_{C\beta}|$ resonances can clearly be seen in the spectrum instead.

In Fig. 7, the ZQ-spectra and DQ-spectra of ubiquitin are compared with a MIRROR-SQ spectrum optimized for C_α–C' transfer. Both MQ–SQ spectra profit from the lack of multiplet-lines due to the absence of the *J*-splitting in the MQ dimension. In both MQ–SQ spectra 29 resonances are resolved. The C_α–C' resonances of the following residues are resolved in both MQ–SQ spectra M1, I3, V5, I13, T14, L15, E18, P19, T22, V26, K27, A28, K29, K33, E34, P37, P38, G53, T55, L56, D58, N60, I61, S65, Y66, H68. The resonances T12 and L43 are resolved only in the 2D ZQ–SQ spectrum, whereas, the resonances I23 and I36 are resolved only in the 2D DQ–SQ spectrum.

Table 1 lists the SQ, DQ, and ZQ line widths from the experimental spectra of U-^{13}C, ^{15}N labeled ubiquitin (Fig. 7). It was found that the line width in the indirect dimension of both the ZQ–SQ and DQ–SQ experiment corresponded to more than the sum of the SQ line widths. The line widths were taken from traces out of the 2D spectrum. Furthermore, no sign of correlated disorder [45] of shifts of spins within the same amino acid was observed in the SQ–SQ and DQ–SQ spectra (the ZQ–SQ spectra are expected to be insensitive to such disorder). This has also been noted for spider dragline silk [54]. The line width in the MQ dimension in this system is thus expected to be determined predominantly by the less-than-perfect decoupling of the protons. Numerical simulations were performed to determine both the ZQ and DQ line widths in C–CH_2 systems under cw decoupling, with all dipolar couplings and CSA tensors included and a random-field relaxation applied to the protons in Liouville space [55] in order to obtain a more realistic behavior of the spin system. This simple model system confirmed the experimental result that the proton-dominated residual line width in the ZQ or DQ dimension is indeed roughly the sum of the SQ line widths.

Table 1
Experimental determined line width (full width at half maximum) measured in ubiquitin. Compared are the ZQ and DQ line widths to the respectively SQ line widths.

Amino acid	$\Delta^{ZQ}_{COC\alpha}$ (ppm)	Δ^{ZQ}_{CO} (ppm)	$\Delta^{ZQ}_{C\alpha}$ (ppm)	$\Delta^{DQ}_{COC\alpha}$ (ppm)	Δ^{DQ}_{CO} (ppm)	$\Delta^{DQ}_{C\alpha}$ (ppm)
Val26	0.68	0.26	0.29	0.56	0.22	0.22
Pro19	0.7	0.38	0.40	0.72	0.26	0.32
Ser65	0.85	0.28	0.42	0.7	0.19	0.29
Ile3	0.68	0.29	0.32	0.79	0.35	0.35
Met1	0.69	0.33	0.35	0.89	0.23	0.29
His68	0.71	0.29	0.33	1.04	0.25	0.25
Asn60	0.86	0.43	0.43	0.8	0.31	0.28
Glu18	0.8	0.28	0.34	0.8	0.28	0.34
Ala28	0.76	0.33	0.36	0.75	0.29	0.31
Glu34	0.73	0.3	0.31	0.63	0.31	0.28
Leu56	0.46	0.32	0.32	0.64	0.29	0.29
Lys27	0.65	0.32	0.35	0.67	0.25	0.27
Lys29	0.67	0.28	0.29	0.68	0.25	0.27
Ile13	0.81	0.27	0.27	0.73	0.29	0.29
Ile61	0.85	0.31	0.34	0.95	0.28	0.29
Val5	0.74	0.31	0.31	0.99	0.29	0.32
Thr55	0.86	0.29	0.29	0.84	0.29	0.29
Thr22	0.86	0.29	0.32	0.85	0.28	0.28
Lys33	0.75	0.31	0.35	0.69	0.23	0.22
Asp58	0.7	0.34	0.33	0.78	0.33	0.26
Leu15	0.71	0.31	0.31	0.67	0.22	0.25
Pro37	0.86	0.32	0.32	0.71	0.33	0.33
Gly53	0.9	0.29	0.26	0.73	0.26	0.28

5. Conclusions

High-resolution ZQ–SQ solid-state NMR correlation experiments of spin-½ nuclei under MAS were implemented using either dipolar-coupling based sequences like SR6$^2_6$ (efficiency about 46% for a two-spin model system) or *J*-coupling based sequences like POST-C9$^1_6$ with an efficiency of about 90%. The higher efficiency in the *J*-coupling based ZQ sequences is predominantly a consequency of the isotropic nature of the *J* interaction that allows, in principle, for complete transfer while the powder-averaging of the dipolar interaction sets a theoretical maximum of 73%. Numerical simulations of basic *J*-coupled systems gave a good agreement with our experimental data, with intensities observed in the ZQ–SQ correlation experiments matching the corresponding *J*-coupling networks of the model compounds. We have applied the ZQ–SQ experiment to the more challenging system of ubiquitin and achieved an efficiency of 50% for the C_α–C' transitions. The resulting spectra had good signal dispersion and resolution comparable to DQ–SQ and SQ–SQ correlation spectra. Efficient generation of C_α–C_β ZQ transitions did however not work under decoupling fields acceptable for protein samples.

Optimized heteronuclear proton decoupling during ZQ excitation and reconversion is a critically important factor in determining the efficiency of the ZQ generation. The optimum rf-field amplitude of the proton decoupling was found to depend strongly on the MAS frequency and the pulse sequence used. Using the highest possible rf-field amplitude does not necessarily give the highest ZQ efficiencies and an experimental optimization of the rf fields is required. For high MAS frequencies reasonable ZQ efficiency can also be achieved for some spin systems without proton decoupling. For ubiquitin, C_α–C' correlations proved easy to excite under these conditions while C_α–C_β were excited very poorly. The heteronuclear dipolar couplings to the proton network was also found to be the dominant factor for the line widths in both ZQ and DQ dimensions.

Acknowledgments

We thank Herbert Zimmermann, MPI für medizinische Forschung Heidelberg, for synthesizing the glycine ethyl ester, and Ingo Scholl for the MIRROR spectrum. This work was supported by the Swiss National Science Foundation and the ETH through the ETHIRA grant system.

References

[1] R.R. Ernst, Nuclear-magnetic-resonance fourier-transform spectroscopy (Nobel Lecture), Angew. Chem.-Int. Ed. Engl. 31 (1992) 805–823.
[2] N.M. Szeverenyi, M.J. Sullivan, G.E. Maciel, Observation of spin exchange by two-dimensional fourier transform 13C cross polarization-magic-angle spinning, J. Magn. Reson. 47 (1982) 462–475.
[3] D.P. Weitekamp, Time-domain multiple-quantum NMR, Adv. Magn. Reson. 11 (1983) 111–274.
[4] G. Bodenhausen, Multiple-quantum NMR, Prog. Nucl. Magn. Reson. Spectrosc. 14 (1980) 137–173.
[5] J. Jeener, B.H. Meier, P. Bachmann, R.R. Ernst, Investigation of exchange processes by two-dimensional NMR spectroscopy, J. Chem. Phys. 71 (1979) 4546.
[6] T. Manolikas, T. Herrmann, B.H. Meier, Protein structure determination from C-13 spin-diffusion solid-state NMR spectroscopy, J. Am. Chem. Soc. 130 (2008) 3959–3966.
[7] J. Boyd, C.M. Dobson, C. Redfield, Correlation of proton chemical-shifts in proteins using two-dimensional double-quantum spectroscopy, J. Magn. Reson. 55 (1983) 170–176.
[8] S. Luca, M. Baldus, Enhanced spectral resolution in immobilized peptides and proteins by combining chemical shift sum and difference spectroscopy, J. Magn. Reson. 159 (2002) 243–249.
[9] A. Wokaun, R.R. Ernst, Selective detection of multiple quantum transitions in NMR by two-dimensional spectroscopy, Chem. Phys. Lett. 52 (1977) 407–412.
[10] R. Verel, T. Manolikas, A.B. Siemer, B.H. Meier, Improved resolution in 13C solid-state spectra through spin-state-selection, J. Magn. Reson. 184 (2007) 322–329.

[11] L. Duma, S. Hediger, A. Lesage, L. Emsley, Spin-state selection in solid-state NMR, J. Magn. Reson. 164 (2003) 187–195.
[12] L. Duma, S. Hediger, B. Brutscher, A. Bockmann, L. Emsley, Resolution enhancement in multidimensional solid-state NMR spectroscopy of proteins using spin-state selection, J. Am. Chem. Soc. 125 (2003) 11816–11817.
[13] M. Baldus, B.H. Meier, Total correlation spectroscopy in the solid state. The use of scalar couplings to determine the through-bond connectivity, J. Magn. Reson. A 121 (1996) 65–69.
[14] M. Baldus, R.J. Iuliucci, B.H. Meier, Probing through-bond connectivities and through-space distances in solids by magic-angle-spinning nuclear magnetic resonance, J. Am. Chem. Soc. 119 (1997) 1121–1124.
[15] E.H. Hardy, R. Verel, B.H. Meier, Fast MAS total through-bond correlation spectroscopy, J. Magn. Reson. 148 (2001) 459–464.
[16] E.H. Hardy, A. Detken, B.H. Meier, Fast-MAS total through-bond correlation spectroscopy using adiabatic pulses, J. Magn. Reson. 165 (2003) 208–218.
[17] M.G. Colombo, B.H. Meier, R.R. Ernst, Rotor-driven spin diffusion in natural-abundance ^{13}C spin systems, Chem. Phys. Lett. 146 (1988) 189–196.
[18] M.H. Levitt, D.P. Raleigh, F. Creuzet, R.G. Griffin, Theory and simulations of homonuclear spin pair systems in rotating solids, J. Chem. Phys. 92 (1990) 6347–6364.
[19] D.P. Raleigh, M.H. Levitt, R.G. Griffin, Rotational resonance in solid-state NMR, Chem. Phys. Lett. 146 (1988) 71–76.
[20] D.K. Sodickson, M.H. Levitt, S. Vega, R.G. Griffin, Broad-band dipolar recoupling in the nuclear-magnetic-resonance of rotating solids, J. Chem. Phys. 98 (1993) 6742–6748.
[21] A.E. Bennett, J.H. Ok, R.G. Griffin, S. Vega, Chemical-shift correlation spectroscopy in rotating solids – radio frequency driven dipolar recoupling and longitudinal exchange, J. Chem. Phys. 96 (1992) 8624–8627.
[22] M. Baldus, M. Tomaselli, B.H. Meier, R.R. Ernst, Broad-band polarization-transfer experiments for rotating solids, Chem. Phys. Lett. 230 (1994) 329–336.
[23] M. Baldus, B.H. Meier, Broadband polarization transfer under magic-angle spinning: application to total through-space-correlation NMR spectroscopy, J. Magn. Reson. 128 (1997) 172–193.
[24] A. Brinkmann, J. Schmedt auf der Günne, M.H. Levitt, Homonuclear zero-quantum recoupling in fast magic-angle spinning nuclear magnetic resonance, J. Magn. Reson. 156 (2002) 79–96.
[25] M.H. Levitt, Symmetry-based pulse sequences in magic-angle spinning solid-state NMR, in: J.W. Sons (Ed.), Encyclopedia of Nuclear Magnetic Resonance, 2002, pp. 165–196.
[26] N.C. Nielsen, H. Bildsøe, H.J. Jakobsen, M.H. Levitt, Double-quantum homonuclear rotary resonance – efficient dipolar recovery in magic-angle-spinning nuclear resonance, J. Chem. Phys. 101 (1994) 1805–1812.
[27] R. Verel, M. Ernst, B.H. Meier, Adiabatic dipolar recoupling in solid-state NMR: the DREAM scheme, J. Magn. Reson. 150 (2001) 81–99.
[28] R. Tycko, G. Dabbagh, Nuclear-magnetic-resonance crystallography – molecular orientational ordering in 3 forms of solid methanol, J. Am. Chem. Soc. 113 (1991) 3592–3593.
[29] W. Sommer, J. Gottwald, D.E. Demco, H.W. Spiess, Dipolar heteronuclear multiple-quantum NMR-spectroscopy in rotating solids, J. Magn. Reson. A 113 (1995) 131–134.
[30] M. Feike, D.E. Demco, R. Graf, J. Gottwald, S. Hafner, H.W. Spiess, Broadband multiple-quantum NMR spectroscopy, J. Magn. Reson. A 122 (1996) 214–221.
[31] Y.K. Lee, N.D. Kurur, M. Helmle, O.G. Johannessen, N.C. Nielsen, M.H. Levitt, Efficient dipolar recoupling in the NMR of rotating solids – a sevenfold symmetrical radiofrequency pulse sequence, Chem. Phys. Lett. 242 (1995) 304–309.
[32] M. Hohwy, H.J. Jakobsen, M. Eden, M.H. Levitt, N.C. Nielsen, Broadband dipolar recoupling in the nuclear magnetic resonance of rotating solids: a compensated C7 pulse sequence, J. Chem. Phys. 108 (1998) 2686–2694.
[33] C.M. Rienstra, M.E. Hatcher, L.J. Mueller, B.Q. Sun, S.W. Fesik, R.G. Griffin, Efficient multispin homonuclear double-quantum recoupling for magic-angle spinning NMR: C-13–C-13 correlation spectroscopy of U–C-13-erythromycin A, J. Am. Chem. Soc. 120 (1998) 10602–10612.
[34] A. Brinkmann, M. Eden, M.H. Levitt, Synchronous helical pulse sequences in magic-angle spinning nuclear magnetic resonance: double quantum recoupling of multiple-spin systems, J. Chem. Phys. 112 (2000) 8539–8554.
[35] M. Carravetta, M. Eden, X. Zhao, A. Brinkmann, M.H. Levitt, Symmetry principles for the design of radiofrequency pulse sequences in the nuclear magnetic resonance of rotating solids, Chem. Phys. Lett. 321 (2000) 205–215.
[36] M. Hohwy, C.M. Rienstra, C.P. Jaroniec, R.G. Griffin, Fivefold symmetric homonuclear dipolar recoupling in rotating solids: application to double quantum spectroscopy, J. Chem. Phys. 110 (1999) 7983–7992.
[37] C.E. Hughes, S. Luca, M. Baldus, Radio-frequency driven polarization transfer without heteronuclear decoupling in rotating solids, Chem. Phys. Lett. 385 (2004) 435–440.
[38] I. Marin-Montesinos, D.H. Brouwer, G. Antonioli, W.C. Lai, A. Brinkmann, M.H. Levitt, Heteronuclear decoupling interference during symmetry-based homonuclear recoupling in solid-state NMR, J. Magn. Reson. 177 (2005) 307–317.
[39] D.M. Gregory, D.J. Mitchell, J.A. Stringer, S. Kiihne, J.C. Shiels, J. Callahan, M.A. Mehta, G.P. Drobny, Windowless dipolar recoupling – the detection of weak dipolar couplings between spin 1/2 nuclei with large chemical-shift anisotropies, Chem. Phys. Lett. 246 (1995) 654–663.
[40] T.J. Norwood, Absorption-mode phase-sensitivity zero-quantum-coherence correlation spectroscopy, J. Magn. Reson. A 105 (1993) 193–203.
[41] A.E. Bennett, C.M. Rienstra, M. Auger, K.V. Lakshmi, R.G. Griffin, Heteronuclear decoupling in rotating solids, J. Chem. Phys. 103 (1995) 6951–6958.
[42] T.P. Spaniol, A. Kubo, T. Terao, Resolution enhancement of magic-angle spinning NMR spectra for paramagnetic solids by zero-quantum NMR, Mol. Phys. 96 (1999) 827–834.
[43] Y. Ishii, J. Ashida, T. Terao, 13C–1H dipolar recoupling dynamics in 13C multiple-pulse solid-state NMR, Chem. Phys. Lett. 246 (1995) 439–445.
[44] D. Sakellariou, S.P. Brown, A. Lesage, S. Hediger, M. Bardet, C.A. Meriles, A. Pines, L. Emsley, High-resolution NMR correlation spectra of disordered solids, J. Am. Chem. Soc. 125 (2003) 4376–4380.
[45] S. Cadars, A. Lesage, L. Emsley, Chemical shift correlations in disordered solids, J. Am. Chem. Soc. 127 (2005) 4466–4476.
[46] S. Spera, A. Bax, Empirical correlation between protein backbone conformation and C-alpha and C-beta ^{13}C nuclear-magnetic-resonance chemical-shifts, J. Am. Chem. Soc. 113 (1991) 5490–5492.
[47] A. Samoson, T. Tuherm, J. Past, Ramped-speed cross polarization MAS NMR, J. Magn. Reson. 149 (2001) 264–267.
[48] H. Geen, R. Freeman, Band-selective radiofrequency pulses, J. Magn. Reson. 93 (1991) 93–141.
[49] J.D. van Beek, MatNMR: a flexible toolbox for processing, analyzing and visualizing magnetic resonance data in Matlab(R), J. Magn. Reson. 187 (2007) 19–26.
[50] J. Sass, F. Cordier, A. Hoffmann, A. Cousin, J.G. Omichinski, H. Lowen, S. Grzesiek, Purple membrane induced alignment of biological macromolecules in the magnetic field, J. Am. Chem. Soc. 121 (1999) 2047–2055.
[51] S.A. Smith, T.O. Levante, B.H. Meier, R.R. Ernst, Computer-simulations in magnetic-resonance – an object-oriented programming approach, J. Magn. Reson. A 106 (1994) 75–105.
[52] I. Scholz, M. Huber, T. Manolikas, B.H. Meier, M. Ernst, MIRROR recoupling and its application to spin diffusion under fast magic-angle spinning, Chem. Phys. Lett. 460 (2008) 278–283.
[53] A. Detken, E.H. Hardy, M. Ernst, B.H. Meier, Simple and efficient decoupling in magic-angle spinning solid-state NMR: the XiX scheme, Chem. Phys. Lett. 356 (2002) 298–304.
[54] I. Marcotte, J.D. van Beek, B.H. Meier, Molecular disorder and structure of spider dragline silk investigated by two-dimensional solid-state NMR spectroscopy, Macromolecules 40 (2007) 1995–2001.
[55] M. Ernst, H. Zimmermann, B.H. Meier, A simple model for heteronuclear spin decoupling in solid-state NMR, Chem. Phys. Lett. 317 (2000) 581–588.